Control of Exciton Fluxes in an Excitonic Integrated Circuit

Alex A. High,[1] Ekaterina E. Novitskaya,[1] Leonid V. Butov,[1]* Micah Hanson,[2] Arthur C. Gossard[2]

Efficient signal communication uses photons. Signal processing, however, uses an optically inactive medium, electrons. Therefore, an interconnection between electronic signal processing and optical communication is required at the integrated circuit level. We demonstrated control of exciton fluxes in an excitonic integrated circuit. The circuit consists of three exciton optoelectronic transistors and performs operations with exciton fluxes, such as directional switching and merging. Photons transform into excitons at the circuit input, and the excitons transform into photons at the circuit output. The exciton flux from the input to the output is controlled by a pattern of the electrode voltages. The direct coupling of photons, used in communication, to excitons, used as the device-operation medium, may lead to the development of efficient exciton-based optoelectronic devices.

The advancement of signal processing and communication has led to the development of optoelectronic and all-optical circuits, which expand signal processing into an optically active medium (*1*, *2*). Semiconductor-based optoelectronic components are of particular interest because they can be integrated into circuits in a way similar to that of electronic integrated circuits. The advances in this direction include in particular the development of an optoelectronic transistor (*3*) and compact microring (*4*) and Mach-Zehnder (*5*) modulators. The latter devices have achieved switching speeds exceeding several gigahertz with active-region dimensions in the range of 10 to 100 μm (*4*, *5*). The development of optoelectronic devices with still smaller dimensions is attractive because this would permit a high packing density, one of the key advantages of electronic integrated circuits.

Excitons, bound pairs of electrons and holes, have been used in the development of semiconductor-based optoelectronic devices, which utilize an optically active medium. The optoelectronic devices operating with excitons include modulators (*6*), storage devices (*7*, *8*), field-gradient devices (*9*, *10*), and transistors (*11*). Yet, integration of these optoelectronic devices into circuits, a crucial requirement for signal processing, has remained an open challenge. We demonstrated an excitonic integrated circuit (EXIC), which can be used to perform operations on photonic signals such as switching and merging.

Because an exciton can be described as a hydrogen-like bosonic particle (*12*), the control of exciton fluxes opens a pathway to the study of excitons in controllable potential profiles—a bosonic counterpart of electronic mesoscopics, the field concerning electron transport in potential profiles.

Exploiting excitonic transport in devices requires the ability to control the exciton energy by an applied gate voltage, and also requires a sufficiently long exciton lifetime so that the excitons can travel over large distances exceeding the device dimensions. A regular exciton is a neutral particle without a built-in dipole moment. It is therefore only weakly sensitive to an applied electric field. Furthermore, its lifetime in a direct-gap semiconductor is typically less than a nanosecond, allowing it to travel only a small distance before it recombines. It is of particular interest to study the mesoscopics of cold excitons analogously to the mesoscopics of electrons, in which interesting physics emerges at low temperatures. However, the same rapid electron-hole recombination, which does not allow regular excitons to travel over large distances, also does not allow them to reach low temperatures within their short lifetime.

An indirect exciton is composed of an electron and a hole, which are confined in spatially separated layers and can be formed in coupled quantum wells (CQWs) (Fig. 1A). The indirect excitons in CQWs are dipoles, with the dipole moment close to the distance between the QW centers (d). Therefore, an electric field F_z perpendicular to the QW plane results in the exciton energy shift $\delta E = eF_z d$ (Fig. 1B). The laterally modulated electrode voltage $V(x,y)$ creates a laterally modulated electric field $F_z(x,y)$ and, in turn, a lateral relief of the exciton energy $\delta E(x,y) = eF_z(x,y)d \propto V(x,y)d$. Shaping of $V(x,y)$ by an appropriate patterning of electrodes allows the creation of virtually any required in-plane potential profiles for excitons. Particular cases include potential gradients (*9*, *10*), one-dimensional (*13*–*16*) and two-dimensional (*17*) lateral lattices, and traps (*17*–*19*). Furthermore, changing the applied electrode voltage $V(x,y)$ allows the in situ control of the in-plane potential on a time scale much shorter than the exciton lifetime (*11*).

Because of the spatial separation between the electron and hole layers, the lifetime of the indirect excitons exceeds by orders of magnitude the lifetime of regular excitons and varies typically from 10 ns to 10 μs. The indirect excitons can travel over large distances of tens and hundreds of micrometers within their lifetime (*9*–*11*, *20*–*24*), distances for which devices can be readily patterned.

Furthermore, because of their long lifetime and high cooling rate (*25*), the indirect excitons can cool to low temperatures close to the lattice temperature. Previous studies (*26*) have shown that the temperature of indirect excitons (T_X), exceeds the lattice temperature (T_L) by only a few

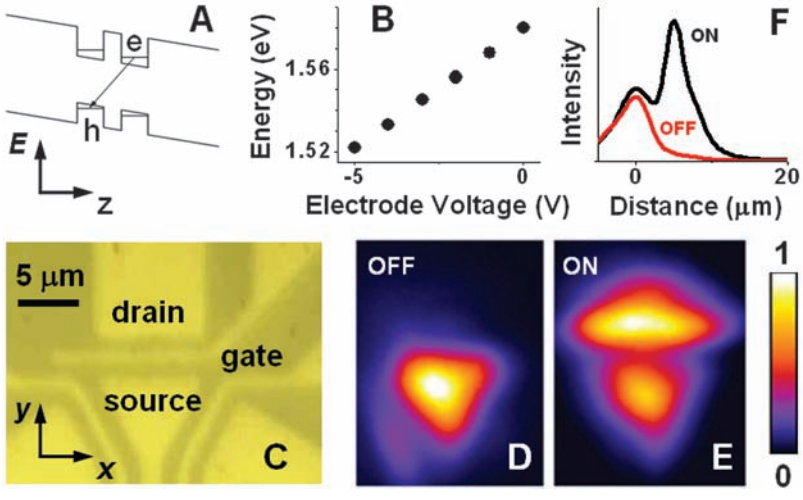

Fig. 1. Principle and operation of the EXOT. (**A**) Energy-band diagram of the CQW structure. e, electron; h, hole. (**B**) Control of the energy of the indirect excitons by gate voltage. (**C** to **E**) Realization of the EXOT. (C) Electrode pattern. [(D) and (E)] Emission of the EXOT in off (D) and on (E) states. The excitons are excited in the source electrode. The energy gradient for the indirect excitons from the source toward the drain is created by the electrode voltages $V_{source} = -1.5$ V and $V_{drain} = -2.5$ V. The exciton flux is controlled by the gate electrode: $V_{gate} = 0$ for the off state, and $V_{gate} = -3$ V for the on state. (**F**) Emission intensity along the exciton flux for off (red line) and on (black line) regimes [which correspond to the false-color images in (D) and (E)].

[1]Department of Physics, University of California at San Diego, La Jolla, CA 92093–0319, USA. [2]Department of Materials, University of California at Santa Barbara, Santa Barbara, CA 93106–5050, USA.

*To whom correspondence should be addressed. E-mail: lvbutov@physics.ucsd.edu

kelvin in the area of the laser excitation. In this work, the experimental data were taken at T_L = 1.4 K. For this lattice temperature, $T_X \sim 3$ K in the laser excitation area (*26*). In the course of exciton transport to a few micrometers away from the laser excitation area, the indirect excitons can cool down even further and essentially reach the lattice temperature (*26*). In the temperature range of a few kelvin, the exciton thermal de Broglie wavelength $\lambda_{dB} = \sqrt{2\pi\hbar^2/(mk_BT_X)} \sim 0.1$ μm (where $\hbar^2$ is the Planck constant, m is the exciton effective mass, and k_B is the Boltzmann constant) and the exciton coherence length approaches a micrometer (*27*), length scales that are not much smaller than the device size (Figs. 1 to 3). This relation between the lengths is typical for mesoscopic devices. Although the ability of indirect excitons to cool to low temperatures is not necessary for optoelectronic applications, it makes them useful for studying the mesoscopics of bosons.

Devices based on excitons can only be operational at temperatures in which the excitons exist. This temperature range is determined to be roughly below E_X/k_B, where E_X is the exciton-binding energy (*28*). For indirect excitons formed in a $Al_{0.33}Ga_{0.67}As/GaAs$ CQW structure with d = 12 nm, E_X/k_B is on the order of 40 K (*29*). However, E_X can be varied by choosing different semiconductor materials and different structure parameters. For instance, in wide-bandgap semiconductor materials, E_X/k_B approaches the room temperature. The operation temperature is also limited by the possibility of spatial separation of electrons and holes by the applied electric field: The energy eF_zd should be higher than k_BT [in the sample described in this paper, eF_zd reached 50 meV; that is, $eF_Zd/k_B \sim 600$ K (Fig. 1B)]. Efficient device operation requires high-quality samples with a low, nonradiative recombination rate.

We built an EXIC that consisted of three exciton optoelectronic transistors (EXOTs). The EXIC was realized in a $Al_{0.33}Ga_{0.67}As/GaAs$ CQW structure (*30*). Both the operation principle and geometry of the EXOT mirror those of an electronic field-effect transistor (FET). Both the FET and EXOT are three-terminal devices in which the electron (FET) or exciton (EXOT) flux between two electrodes is controlled by the voltage applied to the third electrode. A transistor can operate in the modulation (switching) mode or amplification mode, depending on the loading scheme. In our circuit, the EXOTs operate in the former mode. The excitons are excited in the source electrode and travel from the input (source) to the output (drain) because of the potential energy gradient $\delta E \sim e(F_{zd} - F_{zs})d \propto (V_d - V_s)d$ created by the difference in the source voltage V_s and drain voltage V_d. The exciton flux from the source to the drain is controlled by a gate voltage V_g, which controls an energy barrier for the indirect excitons in the region of the gate electrode. The exciton emission rate can be controlled by F_z, and therefore the optical readout can be driven by applying a voltage pulse to the output electrode; however, this was not used in the demonstration described here. The emission image for one of the EXOTs in both the off state and on state is shown in Fig. 1, D and E, respectively. Figure 1F shows that the on/off ratio of the signal integrated over the output exceeds 30. The distance between the source and drain for the EXOT is 3 μm (limited by the resolution of the lithography used for the sample processing). The EXOT spatial dimensions may be able to be reduced below 1 μm, thereby permitting a high

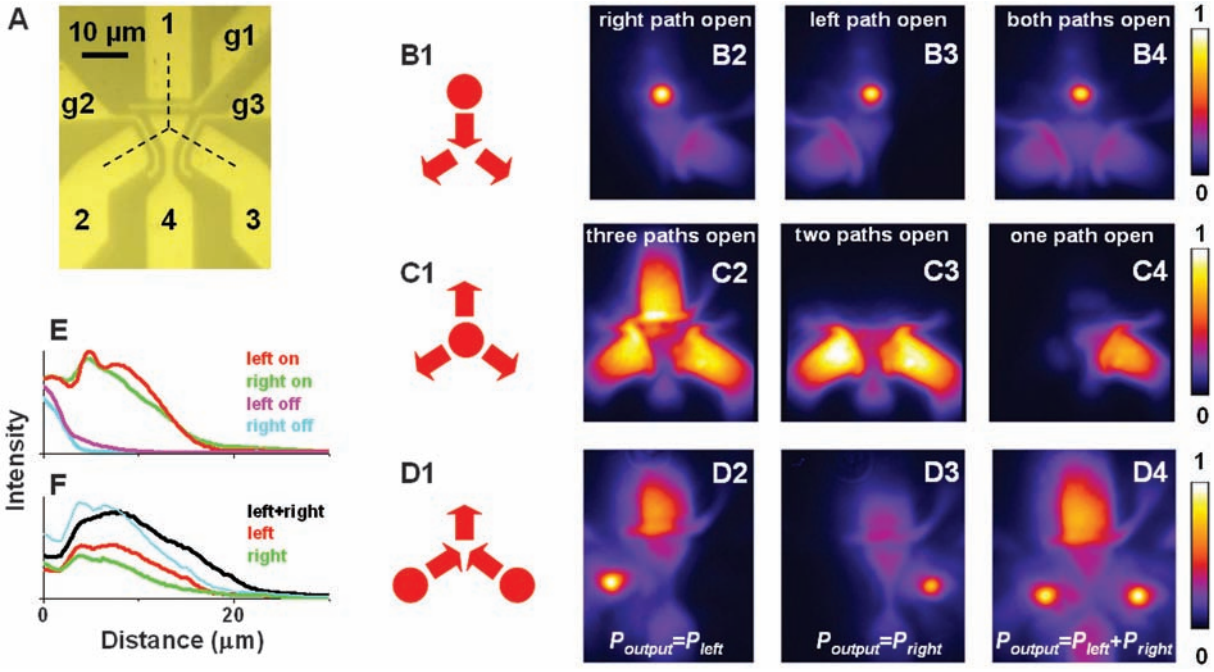

Fig. 2. Operation of the excitonic integrated circuit. (**A**) Electrode pattern. (**B1**, **C1**, and **D1**) Schematics for photoexcitation spots (points) and fluxes (arrows) of indirect excitons in the circuit. (**B2** to **B4**) Demonstration of the directional switch. The excitons are photoexcited at electrode 1. The energy gradient for the indirect excitons from electrode 1 toward electrodes 2 and 3 is created by the electrode voltages $V_1 = -0.5$ V, $V_4 = -1.5$ V, $V_2 = V_3 = -2.5$ V, and $V_{g1} = -2$ V. The exciton fluxes are directed by electrodes g2 and g3: (B2), $V_{g2} = 0$, $V_{g3} = -3$ V; (B3), $V_{g2} = -3$ V, $V_{g3} = 0$; and (B4), $V_{g2} = -3$ V, $V_{g3} = -3$ V. (**C2** to **C4**) Demonstration of the star switch. The excitons are photoexcited at the center. The energy gradient for the indirect excitons from electrode 4 toward electrodes 1 to 3 is created by the electrode voltages $V_1 = V_2 = V_3 = -1.5$ V and $V_4 = -0.5$ V. The exciton fluxes are directed by electrodes g1 to g3: (C2), $V_{g1} = V_{g2} = V_{g3} = -2$ V; (C3), $V_{g1} = 0$ V, $V_{g2} = V_{g3} = -2$ V; and (C4), $V_{g1} = V_{g2} = 0$, $V_{g3} = -2$ V. (**D2** to **D4**) Demonstration of flux merging for indirect excitons. The excitons are photoexcited at electrodes 2 (D2), 3 (D3), or 2 and 3 (D4). The energy gradient for the indirect excitons from electrodes 2 and 3 toward electrode 1 is created by the electrode voltages $V_1 = -2.5$ V, $V_2 = V_3 = -0.5$ V, $V_4 = -1.5$ V, $V_{g1} = -3$ V, and $V_{g2} = V_{g3} = -2$ V. (**E**) Emission intensity along the exciton fluxes [lower dashed lines in (A)] for the left and right paths of the directional switch in on and off regimes [which correspond to the false-color images in (B)]. (**F**) Emission intensity along the exciton flux [top dashed line in (A)] for the left, right, and both paths open of the flux merger [which correspond to the false-color images in (D)]. The experimental combined signal integrated over the output is within 5% of the sum of the signals from the left and right paths (thin blue line).

packing density, one of the key advantages of EXICs.

The device geometry allows the construction of EXICs. For instance, a drain of one EXOT can serve as a source of another EXOT. Figure 2 describes the integrated circuit, in which three EXOTs have a common electrode and form the geometry of a three-beam star. This excitonic integrated circuit can perform several operations with the exciton fluxes, which are determined by the patterns of the exciton photoexcitation and the electrode voltage.

The first scheme in Fig. 2 demonstrates the directional switching of the exciton flux. The excitons are photoexcited at the input of the top EXOT (electrode 1) and travel to the left and right paths (electrodes 2 and 3, respectively) because of the potential energy gradient, which is created by the voltages on electrodes 1 to 4. The exciton flux is controlled by the voltages on the gate electrodes V_{g1}, V_{g2}, and V_{g3}, as demonstrated in Fig. 2B. Opening the right gate and closing the left gate directs the exciton flux to the right path, whereas exchanging V_{g2} and V_{g3} switches the flux direction. The exciton fluxes are visualized by the exciton emission. Figure 2E shows that the on/off ratio of the excitonic directional switch exceeds 50. The typical transported exciton density, estimated from the exciton energy shift [as in (*26*)], is $n \sim 5 \times 10^{10}$ cm^{-2} when the device is open. In turn, the corresponding number of transported excitons $N = nS \sim 10^5$, where S is the area of the exciton cloud at the region of the output electrode.

The second scheme in Fig. 2 demonstrates the directional switching of the exciton flux in a star geometry (Fig. 2C). The excitons are photoexcited at the common electrode at the center of the circuit and travel to the top, left, and right paths because of the potential energy gradient, which is created by the voltages on electrodes 1 to 4. The exciton flux is controlled by V_{g1}, V_{g2}, and V_{g3}, which open or close the corresponding path. Figure 2 demonstrates the directing of the exciton fluxes to three paths (Fig. 2, C2), two paths (Fig. 2, C3), and one path (Fig. 2, C4).

The third scheme in Fig. 2 demonstrates the merging of the exciton fluxes (Fig. 2D). The excitons are photoexcited at electrodes 2 and 3 and travel toward the top electrode because of the potential energy gradient, which is created by the voltages on electrodes 1 to 4. The exciton fluxes from the left and right arms are controlled by V_{g2} and V_{g3}, respectively. The two fluxes flow to the top separately when only one of the paths is open (Fig. 2, D2 and D3) and are combined when both paths are open (Fig. 2, D4). When both paths are open, the circuit implements the optoelectronic sum operation for the exciton fluxes (Fig. 2, D2 to D4). Figure 2F shows that the excitonic flux merger performs the sum operation with a high accuracy: The experimental combined signal integrated over the output is within 5% of the sum of the signals from the left and right paths. The circuit can also implement the all-optical logic AND gate with a one set at a higher level, which is achieved by the combined input signals from both paths ($P_{\text{output-1}} \approx P_{\text{left}} + P_{\text{right}}$), and a zero set at a lower level, which cannot be achieved by the left or right input signal separately ($P_{\text{output-0}} < P_{\text{left}} + P_{\text{right}}$).

The exciton energy as a function of coordinate is presented in Fig. 3. The images demonstrate the excitons' drift down the potential energy gradient created by the pattern of electrode voltages. Previous studies have shown that, in this temperature range and in the presence of a potential energy gradient, exciton transport in a CQW structure can be described by drift and diffusion (*26*).

The circuits perform electronic operations on excitons, which can also be viewed as electronic operations on photons using excitons as intermediate media. Our device operates as a directional switch, star switch, and flux merger. The direct coupling of photons, used in communication, to excitons, used as the device operation medium, may lead to the development of efficient exciton-based optoelectronic devices. The demonstrated control of exciton fluxes opens the possibility of studying excitons in controllable potential profiles. Virtually any in-plane potential relief can be created for excitons by the appropriately designed voltage pattern, including, for instance, traps, quantum point contacts, conveyers, and lattices.

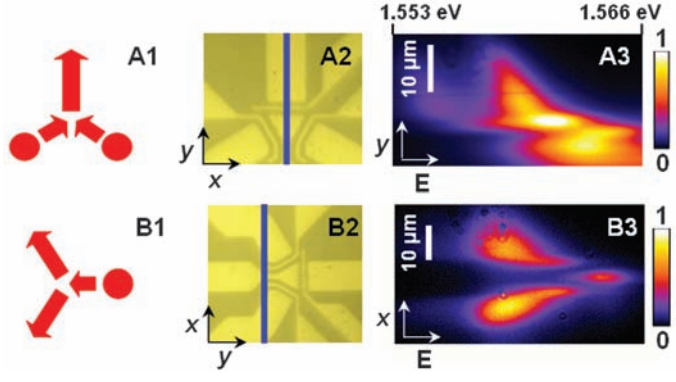

Fig. 3. Indirect exciton flux follows the energy gradient. (**A1**) Schematic for indirect exciton fluxes in the flux merger. (**A2**) *x*-*y* image of the excitonic integrated circuit. (**A3**) Energy–*y*-coordinate image of the indirect exciton flux. The exciton energy was dispersed by the spectrometer; the spectrometer slit position is shown by the blue line in (A2). Applied voltages and excitation spot positions are the same as in Fig. 2, D4. (**B1**) Schematic for indirect exciton fluxes in the directional switch. (**B2**) *y*-*x* image of the excitonic integrated circuit. (**B3**) Energy–*x*-coordinate image of the indirect exciton flux. The spectrometer slit position is shown by the blue line in B2. Applied voltages and excitation spot position are the same as in Fig. 2, B4.

References and Notes

1. H. M. Gibbs, *Optical Bistability: Controlling Light with Light* (Academic Press, New York, 1985).
2. K. Wakita, *Semiconductor Optical Modulators* (Kluwer Academic Publishers, Norwell, MA, 1998).
3. B. F. Aull *et al.*, *Appl. Phys. Lett.* **63**, 1555 (1993).
4. Q. Xu, B. Schmidt, S. Pradhan, M. Lipson, *Nature* **435**, 325 (2005).
5. W. M. J. Green, M. J. Rooks, L. Sekaric, Y. A. Vlasov, *Opt. Express* **15**, 17106 (2007).
6. D. A. B. Miller *et al.*, *Phys. Rev. B* **32**, 1043 (1985).
7. T. Lundstrom, W. Schoenfeld, H. Lee, P. M. Petroff, *Science* **286**, 2312 (1999).
8. A. G. Winbow, A. T. Hammack, L. V. Butov, A. C. Gossard, *Nano Lett.* **7**, 1349 (2007).
9. M. Hagn, A. Zrenner, G. Böhm, G. Weimann, *Appl. Phys. Lett.* **67**, 232 (1995).
10. A. Gartner, A. W. Holleithner, J. P. Kotthaus, D. Schul, *Appl. Phys. Lett.* **89**, 052108 (2006).
11. A. A. High, A. T. Hammack, L. V. Butov, M. Hanson, A. C. Gossard, *Opt. Lett.* **32**, 2466 (2007).
12. L. V. Keldysh, A. N. Kozlov, *Sov. Phys. JETP* **27**, 521 (1968).
13. S. Zimmermann *et al.*, *Phys. Rev. B* **56**, 13414 (1997).
14. S. Zimmermann, A. Wixforth, J. P. Kotthaus, W. Wegscheider, M. Bichler, *Science* **283**, 1292 (1999).
15. J. Krauß *et al.*, *Appl. Phys. Lett.* **85**, 5830 (2004).
16. S. K. Zhang, P. V. Santos, R. Hey, A. Garcia-Cristobal, A. Cantarero, *Appl. Phys. Lett.* **77**, 4380 (2000).
17. A. T. Hammack *et al.*, *J. Appl. Phys.* **99**, 066104 (2006).
18. T. Huber, A. Zrenner, W. Wegscheider, M. Bichler, *Phys. Status Solidi* **166**, R5 (1998).
19. G. Chen *et al.*, *Phys. Rev. B* **74**, 045309 (2006).
20. A. V. Larionov, V. B. Timofeev, J. Hvam, K. Soerensen, *Sov. Phys. JETP* **90**, 1093 (2000).
21. L. V. Butov, A. C. Gossard, D. S. Chemla, *Nature* **418**, 751 (2002).
22. Z. Vörös, R. Balili, D. W. Snoke, L. Pfeiffer, K. West, *Phys. Rev. Lett.* **94**, 226401 (2005).
23. A. L. Ivanov *et al.*, *Europhys. Lett.* **73**, 920 (2006).
24. R. Rapaport, G. Chen, S. H. Simon, *Phys. Rev. B* **73**, 033319 (2006).
25. A. L. Ivanov, P. B. Littlewood, H. Haug, *Phys. Rev. B* **59**, 5032 (1999).
26. A. T. Hammack *et al.*, *Phys. Rev. Lett.* **96**, 227402 (2006).
27. S. Yang, A. T. Hammack, M. M. Fogler, L. V. Butov, A. C. Gossard, *Phys. Rev. Lett.* **97**, 187402 (2006).
28. D. S. Chemla, D. A. B. Miller, P. W. Smith, A. C. Gossard, W. Wiegmann, *IEEE J. Quantum Electron.* **20**, 265 (1984).
29. M. H. Szymanska, P. B. Littlewood, *Phys. Rev. B* **67**, 193305 (2003).
30. Materials and methods are available as supporting material on *Science* Online.

31. This work is supported by the U.S. Army Research Office, the U.S. Department of Energy, and NSF.

Supporting Online Material

www.sciencemag.org/cgi/content/full/1157845/DC1
Materials and Methods
References

17 March 2008; accepted 11 June 2008
Published online 19 June 2008;
10.1126/science.1157845
Include this information when citing this paper.

Control of Exciton Fluxes in an Excitonic Integrated Circuit

Alex A. High, Ekaterina E. Novitskaya, Leonid V. Butov, Micah Hanson and Arthur C. Gossard

Science **321** (5886), 229-231.
DOI: 10.1126/science.1157845originally published online June 19, 2008